AGU ADVANCING EARTH AND SPACE SCIENCES

Water Resources Research®

RESEARCH ARTICLE
10.1029/2023WR035213

Special Collection:
Hydrogeodesy: Understanding changes in water resources using space geodetic observations

High Spatial Resolution in Total Water Storage Variations Inferred From GPS: Case Study in the Great Lakes Watershed, US

Shuo Zheng[1,2], **Zizhan Zhang**[1,2], **Bridget R. Scanlon**[3], **Haoming Yan**[1], **Alexander Y. Sun**[3], **Ashraf Rateb**[3], **and Yan Li**[1]

[1]State Key Laboratory of Geodesy and Earth's Dynamics, Hubei Luojia Laboratory, Innovation Academy of Precision Measurement of Science and Technology, Chinese Academy of Sciences, Wuhan, China, [2]University of Chinese Academy of Sciences, Beijing, China, [3]Bureau of Economic Geology, Jackson School of Geosciences, The University of Texas at Austin, Austin, TX, USA

Key Points:

- A new inversion strategy for Total Water Storage (TWS) was applied to global positioning system (GPS) data by first removing lake water driven load through forward modeling
- GRACE/GFO TWS underestimates spatial patterns of seasonal and long-term TWS fluctuations but coincides with temporal TWS patterns from GPS data
- GPS provides high spatiotemporal resolution in TWS relative to GRACE/GFO and improved understanding water storage dynamics in Great Lakes Watershed

Supporting Information:

Supporting Information may be found in the online version of this article.

Correspondence to:

Z. Zhang,
zzhang@asch.whigg.ac.cn

Citation:

Zheng, S., Zhang, Z., Scanlon, B. R., Yan, H., Sun, A. Y., Rateb, A., & Li, Y. (2024). High spatial resolution in total water storage variations inferred from GPS: Case study in the Great Lakes watershed, US. *Water Resources Research*, *60*, e2023WR035213. https://doi.org/10.1029/2023WR035213

Received 25 JULY 2023
Accepted 29 MAY 2024

Author Contributions:

Conceptualization: Shuo Zheng
Investigation: Shuo Zheng, Zizhan Zhang
Methodology: Shuo Zheng, Zizhan Zhang
Software: Shuo Zheng

Abstract

Assessing spatiotemporal water storage variability in the Great Lakes Watershed (GLW) is critical given its transboundary status impacting both Canada and the United States. Here, we apply a novel inversion strategy to global positioning system (GPS) vertical movements to achieve high spatial resolution total water storage (TWS) variations in GLW through improved processing. The steps are composed of removing load changes driven by the lake water fluctuation by forward modeling, isolating the Great Lakes grids to solve the ill-conditioned problem in inversion, and inverting the GPS residual series to estimate TWS variations on land (TWS_{GPS}). The results show that the regional dense continuous GPS observation network can successfully resolve TWS on land at monthly timescales with 30–45 km spatial resolution. We also could effectively capture fine-scale TWS features than GRACE/GFO mascon products. GRACE/GFO satellites largely underestimate seasonal and long-term TWS spatial fluctuations, but their temporal patterns coincide with those from GPS. The average annual amplitude of TWS_{GPS} on land reaches 82.0 mm, greatly exceeding estimates from GRACE/GFO (~48.0 mm) and composite hydrological model outputs (~62.0 mm). The seasonal groundwater fluctuations inferred from GPS have peak-to-peak amplitudes of ~40 km^3 with the maximum around September. This coincides with that from GRACE/GFO. However, the magnitudes and phases of groundwater storage from GPS vary markedly among the subbasins in GLW, and the different snow and soil moisture amounts measured in each subbasin cause discrepancies among these GPS estimates. This study shows the value of GPS data in spatially downscaling GRACE/GFO data and providing high-resolution output at spatiotemporal scales with low latency.

1. Introduction

The Great Lakes provide drinking water to about 34 million people and water resources is critical for economic development, ecosystem health and weather regulation over the watershed (ELPC, 2019). Total water storage (TWS), including snow, ice, surface water, soil moisture, and groundwater are dynamic components of the hydrologic cycle and play key roles in water storage change and transportation in the Great Lakes Watershed (GLW). Studying long-term and seasonal variations in water storage alongside its spatial distribution characteristics and clarifying the main driving factors are critical for managing regional water resources under climate change.

At present, advanced hydrological simulation and satellite remote sensing products are increasingly used to assess water availability and sustainability. These methods are essential for understanding spatiotemporal changes in terrestrial TWS. Global models, such as global land surface models (LSMs) and global hydrological and water resources models, are widely used to estimate the variability in TWS (Bierkens, 2015) and provide opportunities to assess complex interactions among and transitions in global hydrological signals (Scanlon et al., 2018). However, quantification of TWS from satellite remote sensing are necessary.

The Gravity Recovery and Climate Experiment and GRACE Follow-On (GRACE/GFO) missions opened a new era of global gravity field observations in response to climate and human drivers. GRACE/GFO data are now used globally to monitor storage changes in water cycle (Famiglietti et al., 2015; Tapley et al., 2004, 2019). Tracking changes in TWS by observing changes in Earth's gravity over time at a spatial scale of ~300 km is useful for quantifying global and regional changes in the hydrosphere, cryosphere, and ocean caused by climate change and

Supervision: Zizhan Zhang, Haoming Yan
Validation: Shuo Zheng, Zizhan Zhang, Bridget R. Scanlon, Haoming Yan, Alexander Y. Sun, Ashraf Rateb
Visualization: Shuo Zheng
Writing – original draft: Shuo Zheng
Writing – review & editing: Shuo Zheng, Zizhan Zhang, Bridget R. Scanlon, Haoming Yan, Alexander Y. Sun, Ashraf Rateb, Yan Li

human impacts (Tapley et al., 2019). For example, Huang et al. (2012) used GRACE data to quantify groundwater storage (GWS) changes within the GLW with supplementary surface water storage (SWS) (e.g., lake water, snow, and soil moisture) information and existing glacial isostatic adjustment (GIA) models. However, the coarse spatial resolution of GRACE/GFO data (~300 km), signal leakage during post-processing, and coarse temporal resolution (~1 month) with large latency (~45–60 days) as well as data gaps, make it impossible to provide continuous fine-scale changes in water storage following extreme hydrological events in real time (Jiang et al., 2021; Rodell et al., 2018).

Alternatively, the GPS provides an independent tool for monitoring surface deformation related to the hydrological cycle (Enzminger et al., 2018; Fu et al., 2015). According to the theory of elastic deformation, the Earth deforms elastically in response to changes in the surface load. For example, the loading or unloading of water caused by floods or droughts results in instantaneous vertical and horizontal surface elastic deformation (Heki & Arief, 2022; Milliner et al., 2018). GPS accurately records the vertical motion of the Earth's surface as an elastic response to loading of water with mm-level accuracy (Borsa et al., 2014; Knappe et al., 2019; Young et al., 2021).

Based on the theory of solid Earth elastic loads (Farrel, 1972), an inversion method that relates high-precision surface deformation to hydrological loads has been established to infer daily-to-interannual changes in TWS (Argus et al., 2014, 2017; Overacker et al., 2022). Because crustal deformation decreases rapidly with distance from a surface load center, GPS measurements can naturally resolve fine-scale spatial changes in TWS and compensate for the lack of localized information expressed in satellite-derived gravity observations (Hsu et al., 2020; Jiang et al., 2020; Nahmani et al., 2012). Several kinds of other space geodetic techniques have also been applied to investigate Earth's surface water variations. Such as interferometric synthetic aperture radar (InSAR) and altimetry. The InSAR techniques can measure subsidence associated with water storage change and provide a mean to study TWS on land (White et al., 2022). Satellite altimetry has been proved effective in tracking sea level and lake level change, although it cannot be used to resolve the TWS variations on land. GNSS offers a long-term time series to study the TWS on land. As an additional benefit, GNSS data are, if appropriately analyzed, not so sensitive to atmospheric delays as InSAR.

In GLW, Argus et al. (2020) evaluated the elastic loading deformation driven by increasing levels of the Great Lakes and distinguished multiple causes responsible for long-term and seasonal vertical oscillations in the surrounding land area. Xue et al. (2021) investigated relative contributions of individual hydrological components (e.g., lakes water, snow, soil moisture, and GWS changes in GLW) to the total integrated hydrological loading deformation. Wang et al. (2022) studied interannual fluctuations in water levels in the Great Lakes using GPS and GRACE/GFO observations. These studies assessed the contributions of hydrological loads to the movements of GPS stations in GLW rather than inverting for TWS changes using GPS data. In fact, accurate and high spatial resolution water storage variations in GLW are still unknown, and these results still suffer from substantial ambiguity regarding the magnitude and phase of GWS variations in GLW. Hence, it is critical to obtain accurate water storage variations in GLW using an independent tool.

In this study, we aim at estimating high spatial and temporal resolution TWS changes using GPS data. Here, we extend the approach of Argus et al. (2014) and introduce a novel inversion strategy for GPS data to achieve high spatial resolution TWS. As the first step of our improved processing method, we remove deformation signals caused by the lake water fluctuation by forward modeling and isolate the Great Lakes grids to regularize the ill-conditioned problem of the inversion equation. Then, we quantify long-term and seasonal variations in TWS on land within GLW by integrating data from GPS, GRACE/GFO, and a hydrological model. Finally, we assess the long-term and seasonal fluctuations in GWS associated with potential forcing factors in different GLW subbasins during 2010–2020. Our results highlight the ability of dense continuous GPS network observations in capturing fine-scale spatial variations in TWS and quantifying GWS changes in subbasins in GLW.

2. Data and Processing

2.1. GPS Data and Processing

We collected 616 continuous daily vertical-coordinate time series of GPS stations located in GLW spanning 2010–2020 provided by the Nevada Geodetic Laboratory (NGL, http://geodesy.unr.edu/; Blewitt et al., 2018, 2019). We omitted 225 GPS stations with ≤60% valid data percentages. Then we excluded 23 GPS stations showing poroelastic responses to groundwater pumping, volcanic activity, or oil exploitation (Argus et al., 2020, 2021). Finally, 368 stations were used for the inversion. Nontidal atmospheric loading (NTAL) and nontidal oceanic loading (NTOL) effects were removed from the GPS time series (Figures S1 and S2 in Supporting Information S1). The daily three-dimensional site positions were decomposed into the following components using Equation 1 (Li et al., 2021; Yan et al., 2019; Zhang et al., 2021):

$$x(t) = x_0 + v(t - t_0) + \sum_i \left[S_i\, sin(2pi\omega_i t) + C_i\, cos(2pi\omega_i t)\right] + \sum_k \left[H(t_k - t_e)\right] F_k + r \tag{1}$$

where x_0 is offset bias, v denotes velocity, S_i and C_i represent sine and cosine terms of the annual ($i = 1$) and semiannual ($i = 2$) components, respectively. $H(t_k - t_e)$ is the step function, F_k is the offset resulting from instrumental changes or metadata changes, and r is the residual error. We did not consider coseismic steps because GLW is in a tectonically inactive area. After removing the GIA effects (Peltier et al., 2018), subsidence of GPS stations is primarily a response to increased water storage in GLW. We did not remove linear trends from the time series. We show the daily vertical displacement observed from GPS for four stations from the western, central, and eastern GLW and the corresponding post-processing GPS vertical displacement timeseries in Figure S3 in Supporting Information S1.

2.2. GRACE/GFO Mascon Products

The latest available GRACE/GFO mascon solutions provided by the Center for Space Research at University of Texas, Austin (CSR) were used in this study. The spatial resolution of the CSR RL06 mascon solutions is 0.25° (http://www2.csr.utexas.edu/grace/), and all appropriate corrections (C_{20}, C_{30}, degree-1 and GIA) were applied to the CSR GRACE mascon solutions (Save, 2019; Save et al., 2016). We removed the mean values from the GRACE/GFO mascon solutions (spanning January 2010 through December 2020) to derive the regional TWS anomaly, which we then compared with other water height time series. The RL06 mascon solutions use a newly defined grid with hexagonal tiles. These tiles are split into two along the coastline to minimize leakage between land and ocean signals. No additional Gaussian smoothing, decorrelation filtering, or scaling factors were applied to these new CSR mascon solutions. Leakage of TWS changes into surrounding regions was also evident because the actual dimension of the tiles used in the CSR mascon estimation was ∼330 km, accounting for the possibility that the change within GLW may influence mascons outside its boundary. We included all mascons within 220 km (∼2°) from the boundary of GLW and reallocated the total mascons into the study region to reduce leakage errors (Chen et al., 2016). In this study, we take the root mean square of the residual in TWS after removing the long-term trend, seasonal and interannual signals as the measurement uncertainty in CSR mascon.

2.3. Hydrological Data

In this study, we created a composite hydrological model (CHM) by aggregating snow water storage (SnWS) data from Snow Data Assimilation System (SNODAS) and soil moisture data from the North American Land Data Assimilation System (NLDAS) (Argus et al., 2020). NLDAS contains a series of land surface variables simulated in the Noah land-surface model (LSM) within NLDAS (Mitchell & Kenneth, 2004; Xia et al., 2012). The data are represented on 0.25° × 0.25° latitude-longitude grid (∼13.0 km) and extend from Jan 1979 to present. SNODAS (National Operational Hydrologic Remote Sensing Center, 2004; National Snow and Ice Data Center 2019) data incorporate snow telemetry (SNOTEL) data and provide daily SnWS at a 1-km resolution. We resampled the water storage estimates from both the GRACE/GFO mascon solutions and the CHM product into a 0.5° × 0.5° grid (∼30 × 50 km) to match those inferred from GPS.

2.4. Water Levels in the Great Lakes Watershed

To accurately estimate TWS changes on land in GLW, the effects of lake volume changes must be removed from the vertical displacement data at GPS stations. They also need to be subtracted from TWS changes from GRACE/GFO (TWS_{GRACE}) (Argus et al., 2020; Gronewold et al., 2015; Huang et al., 2012). Monthly water levels are monitored on the Great Lakes by a network of uniformly distributed stations (Figure 1a); these data are provided by Canada's Department of Fisheries and Oceans and by the U.S. National Oceanic and Atmospheric Administration (NOAA). We also confirmed these data sets with satellite altimetry data.

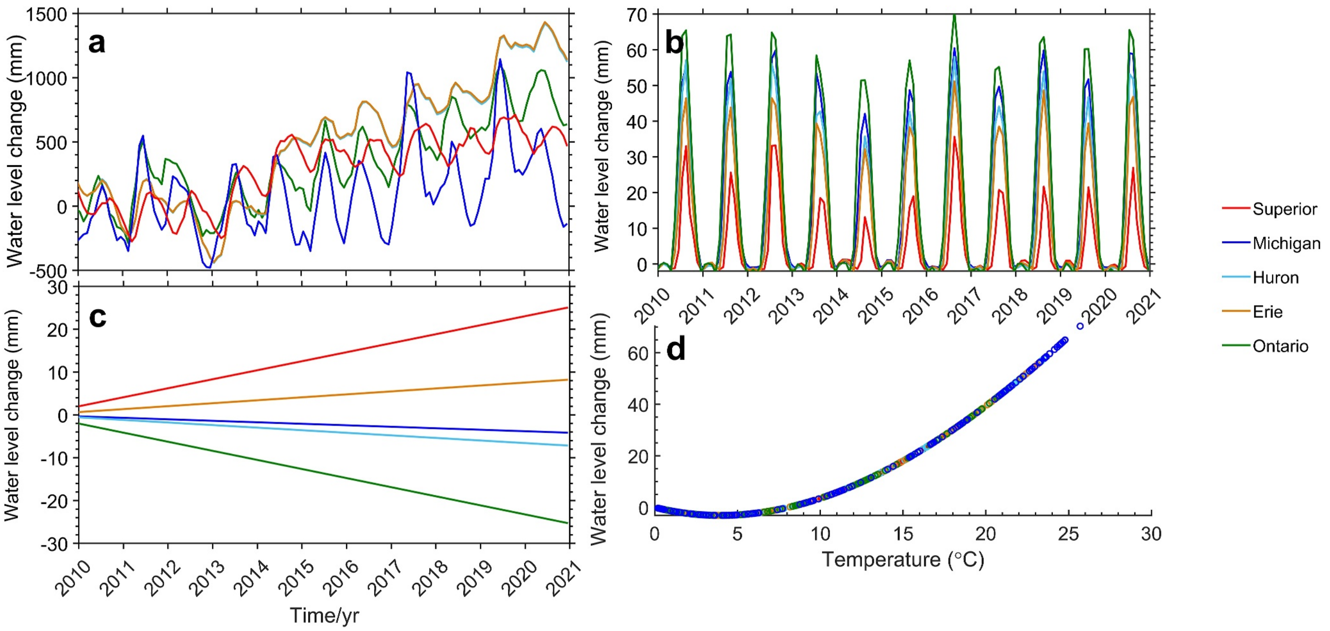

Figure 1. Water level variations in the Great Lakes. (a) Gauged water level changes in the Great Lakes after removing the temperature and glacial isostatic adjustment (GIA) effects from Jan 2010 through Dec 2020. Lake Michigan and Lake Huron have the same water height because they are interconnected. (b) Thermal expansion effect on lake water levels. (c) GIA effect on lake water levels. (d) The scatterplot mapping temperature to water level change.

Lake water levels are affected by temperature changes. When lake water levels are used to estimate SWS changes in GLW, the effects of thermal expansion need to be determined. Here the thermal expansion equation of water was used to estimate them (Meredith, 1975):

$$V_t = \mathrm{V}_0\left(1 - 6.427 \times 10^{-5}\, T + 8.5053 \times 10^{-6}\, T^2 - 6.79 \times 10^{-8}\, T^3\right), \tag{2}$$

where V_0 is water volume at 0°C, T is water temperature, and V_t is water volume at T °C. This equation applies to the temperature range 0–33°C, and water temperatures in the Great Lakes are within this range. Monthly lake-surface temperature data representing the Great Lakes were obtained from the Great Lakes Environmental Research Laboratory (GLERL) lake level products of NOAA. Note that the changes in the surface area of these lakes over 2010–2020 can be ignored (Khandelwal et al., 2022). Hence, we calculated the impact of temperature on the water levels using Equation 2.

The amplitude of lake water level fluctuations caused by thermal expansion recorded the maximum of ~70.0 mm in Lake Erie and the minimum in Lake Superior (average value of 25.0 mm) (Figure 1b). Therefore, the temperature effect on the water levels should be considered in studying seasonal changes of TWS in GLW. Furthermore, the impact of GIA on water level gauges is significant, especially in Lake Superior and Lake Erie (Figure 1c). Therefore, the GIA effect on water level change was removed. The corrected water levels in the Great Lakes are shown in Figure 1a. Figure 1d shows the lake level rise affected by water temperature. Thermal expansion of the Great Lakes needs to be accounted for when the water level is used to estimate SWS.

Following Argus et al. (2020), we applied a two-dimensional Gaussian filter with a 300 km radius to approximate GRACE/GFO measured spatial-time variable gravity signal caused by lake water loading/unloading in GLW. Then we estimated TWS on land by removing Gaussian filtered realization of SWS from $\mathrm{TWS}_{\mathrm{GRACE}}$

3. Materials and Methods

3.1. Study Area

The Great Lakes system, including the five Great Lakes (Superior, Michigan, Huron, Erie, and Ontario), is the world's largest unfrozen surface water system and contains ~21% of the world's surface freshwater covering an area of ~766,100 km^2, with maximum extents ranging from 1,110 km from north to south and ~1,400 km from the west side of Lake Superior to the east side of Lake Ontario. Overall, the GLW comprises 4% of the world's watershed area, and is home to ~30% of the Canadian population and ~10% of the U.S. population (ELPC, 2019; Michalak, 2017). Therefore, water resources management is extremely important in GLW. However, as a result of the complex local climatic conditions, human intervention, and topographical characteristics of GLW, estimating real-time and accurate data on spatiotemporal variability in water storage is challenging (Gronewold et al., 2015). A high-density GPS station network, including 368 stations over GLW area, provides an opportunity to quantify water storage variations for regional water resource management (Figure S4 in Supporting Information S1).

3.2. Methods

3.2.1. Forward Modeling

We calculated the regional surface mass changes by using Green's function to obtain the vertical displacement changes caused by water loading of the Great Lakes at each GPS station following the method of Farrell (1972). Based on the Preliminary Reference Earth Model, the vertical displacement change can be estimated as follows,

$$U(\theta, \varphi) = \iint \Delta m\left(\theta', \varphi'\right) G(\psi) \cos\left(\varphi'\right) d\theta' d\varphi' \tag{3}$$

where Δm represents surface water mass change at cell (θ', φ'), $G(\psi)$ is the vertical Green's function, ψ is the angular distance between cells (θ', φ') and (θ, φ), and U is the GPS observation vector with coordinates (θ, φ).

3.2.2. Inversion Model

The solid Earth deforms elastically in response to mass loadings from water, snow, ice, and the atmosphere. Based on the sensitivity of the solid Earth to the near-field response of the mass loading effect, Green's function can be used to solve the vertical displacement at each GPS station caused by the mass loading at each grid, so TWS variations can be estimated using GPS-measured loading deformation based on the appropriate inversion model (Farrell, 1972; Wahr et al., 2013). We divided the study area into 0.5° × 0.5° grids (~30 × 50 km; Figure S5 in Supporting Information S1) and removed the loading impact of water level changes in the Great Lakes from the GPS data through forward modeling to obtain the residual GPS vertical position time series. In our inversion strategy, the grids over the Great Lakes were excluded, and the residual GPS vertical position time series were used to infer the TWS distribution on land in the study area using the following least squares inversion:

$$min\left\{\|(Ax - b)/\sigma\|^2 + \beta^2 \|L(x)\|^2\right\} \tag{4}$$

where b is the vector of GPS observations, σ is the vector of standard errors, x is the vector of the surface water mass at each cell on land, A is the design matrix consisting of Green's functions relating the surface water mass at a given pixel to the GPS vertical observation, and β is a regularization (damping) parameter. To ensure continuity and smoothness between adjacent grids in the horizontal direction and suppress large and unrealistic water storage changes between neighboring pixels, the Laplacian operator (L) was also applied in our study (Harris & Segall, 1987). The solution for Equation 4 can be written as follows:

$$x = \left(A^T A + \sigma^2 \beta^2 L^T L\right)^{-1} A^T b \tag{5}$$

The value of the damping parameter β was determined using the cross-validation method, resulting in a value of 0.017, as shown in Figure S6 in Supporting Information S1. We use the 2-D discrete Laplacian with the kernels of L2 $\begin{bmatrix} 1 & -2 & 1 \end{bmatrix}$ and L4 $\begin{bmatrix} 0 & 1 & 0 \\ 1 & -4 & 1 \\ 0 & 1 & 0 \end{bmatrix}$. To allow for direct comparisons with the other data sets, we calculated weighted monthly averages from the daily GPS water estimates.

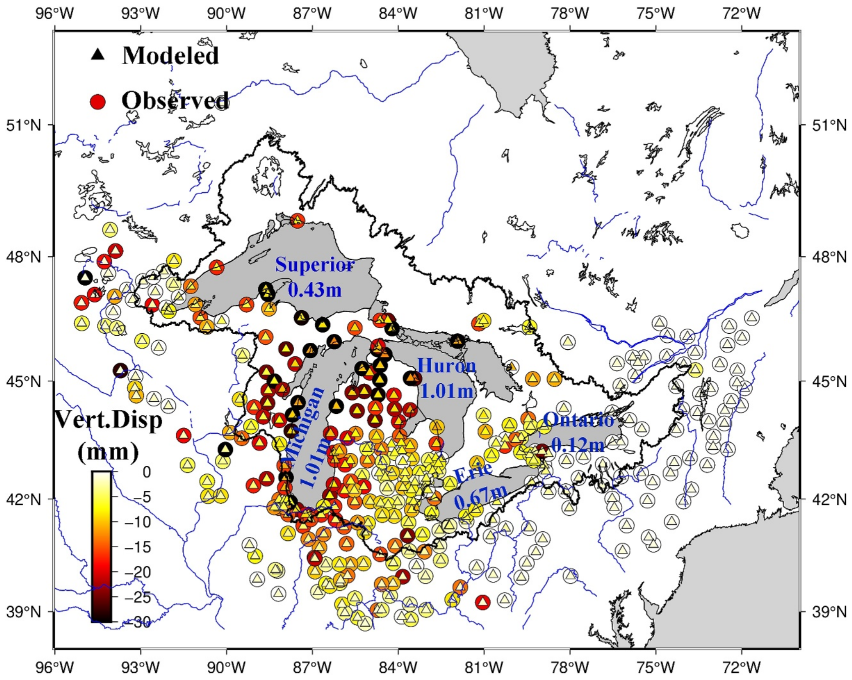

Figure 2. Comparison of observed and modeled vertical displacements at global positioning system (GPS) stations from Jan 2010 through Dec 2020. The circles represent the observed GPS vertical displacements after the glacial isostatic adjustment corrections and the triangles represent the modeled displacements produced by Great Lakes surface water loading from 2010 through 2020. The models and the observations agree in the center and eastern edge of the Great Lakes Watershed, where the model (triangles) and observation (circles) vertical displacements match.

3.2.3. Groundwater Storage Variability

Changes in GWS can be estimated as the residual of the following equation by subtracting changes in the other components of TWS from TWS changes:

$$\Delta GWS = \Delta TWS - \Delta SnWS - \Delta SMS - \Delta SWS \tag{6}$$

where Δ is change, GWS is groundwater storage, SnWS is snow water storage, SMS is soil moisture storage, and SWS is SWS (rivers, lakes, reservoirs, and wetlands). Changes in SnWS and SMS are generally estimated from models (SnWS from SNODAS; CnWS and SMS from NLDAS), and changes in SWS are estimated from water level gauge data.

4. Results

4.1. GIA and Lake Water Loading Effects on GPS Station Displacements

The GIA effect cannot be ignored over GLW (Figure S7 in Supporting Information S1). In the northern part of GLW, the GIA effect leads a large uplift rate at GPS stations, reaching a maximum of 4.6 mm/yr. However, the GIA effect shows a declining trend in the southern part of the basin. To determine long-term trends in TWS, we need to correct the GIA effect for all GPS stations in GLW. To allow for improved comparisons with the GRACE/GFO mascon data, we applied the ICE6G-D model produced by Peltier et al. (2018) to correct the GIA effect on GPS observed displacements.

We first examined the 3-D crustal deformation observed by GPS stations in and surrounding GLW from 2010 to 2020. During this period, most GPS stations at the edge of GLW moved 0.4–4.0 mm toward the Great Lakes responding to the increase of TWS in GLW (Figure S8 in Supporting Information S1), except for few stations that show directional divergence, which may be caused by combined effects of superimposition of local and distant load change. All GPS stations in GLW showed subsidence with the maximum subsidence occurring at a station close to Lake Huron and Lake Michigan (26.0 mm over 2010–2020; Figure 2). Then, we calculated the vertical

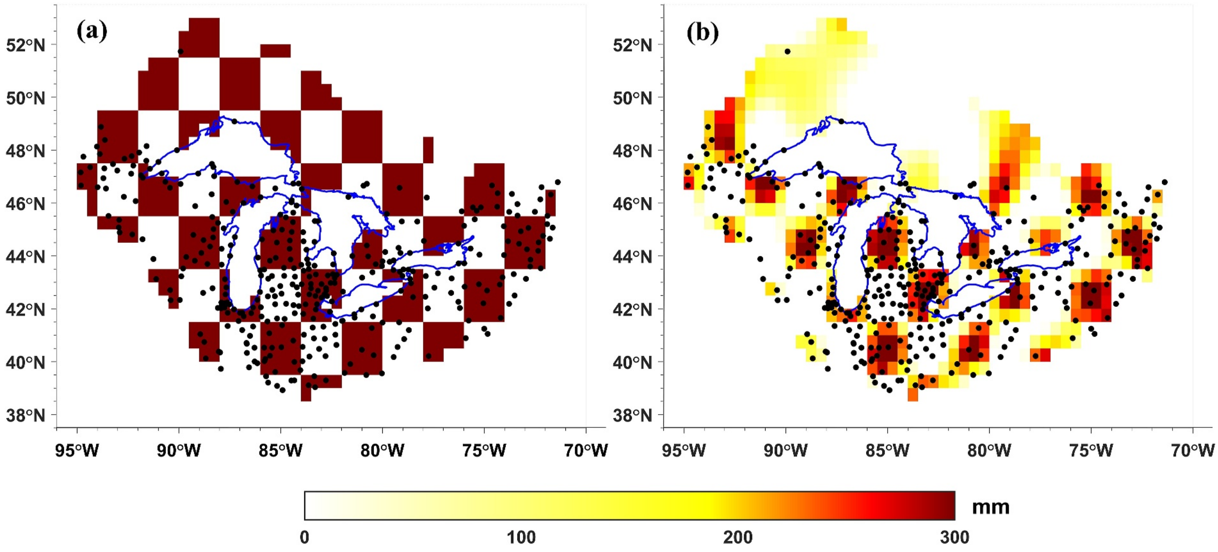

Figure 3. Results of chessboard test. (a) Input water load (in EWH) distribution. (b) Inversion results derived from the synthetic global positioning system data. Pink outline represents the boundary of the Great Lakes Watershed and the orange outline indicates the boundary extended by 2°.

motion of GPS stations in elastic response to lake water load variations (Lake Superior's water level rose 0.43 m, Lake Michigan 1.01 m, Lake Huron 1.01 m, Lake Erie 0.67 m, Lake Ontario 0.12 m) from 2010 to 2020 based on forward modeling method. The modeled results illustrate a clear migration of subsidence across the GLW with the maximum subsidence occurring at the edge of Lake Huron and Lake Michigan (subsidence up to 13.0 mm). Subsidence in stations outside the basin is insignificant and subsidence in stations 200 km away from the GLW can be ignored (<0.3 mm). Comparing observed and modeled displacements at GPS stations (Figure 2), we found that vertical motion observed by GPS cannot be explained only by lake water loading, suggesting we need explore contributions from additional water storage increases on land in GLW. Therefore, we removed the elastic vertical displacements caused by the lake water loading from the GIA corrected GPS timeseries and generated the residual GPS timeseries to infer TWS variations on land in GLW.

4.2. Synthetic Tests of the Inversion Method Using Chessboard Load Mass Sources

To verify the sensitivity and robustness of our inversion strategy, we conducted a synthetic chessboard test. We calculated the vertical crustal displacement in elastic response to a uniform disk load with a radius of 26 km and 1 m water thickness. This disk has the same area as a 0.5° × 0.5° grid (~30 × 50 km) at 43°N in GLW. The calculation shows that the elastic vertical displacement decreases rapidly with increasing distance from the disk center, and is close to zero at about 200 km (~2°) (Figure S9 in Supporting Information S1), so we extended the study domain by 2° in our inversion process. Firstly, we did a forward computation of the vertical displacement at GPS stations responding to the synthetic water loading (Figure 3a) and then converted the synthetic vertical displacement to the water loading distribution on land in GLW (Figure 3b). The inversion result indicates that in most areas of GLW with dense GPS stations, the input water loading distribution can be restored by rates of 80%–85% in magnitude; however, a lower recovery rate (≤40%) occurs in the northwestern region, due to the sparse distribution of GPS stations there. Therefore, to map detailed features in TWS, more continuous GPS stations are required in this region in the future.

To further evaluate the efficiency of our inversion method, we performed another test, firstly inverting GPS observed seasonal amplitudes of surface deformation to the seasonal water loading, then calculating the amplitude of vertical displacements at GPS stations in response to the inverted seasonal water loading through forward modeling. The results indicate that in Michigan and eastern Lake Ontario, seasonal oscillations in TWS are substantial, and maximum TWS_{GPS} amplitude in this area is ~180.0 mm (Figure 4a). However, seasonal oscillations are not obvious in southwestern Ontario, with an average amplitude of ~30 mm. The annual amplitudes measured by GPS agree well with the forward-calculation ($R = 0.86$) and the average annual amplitude difference

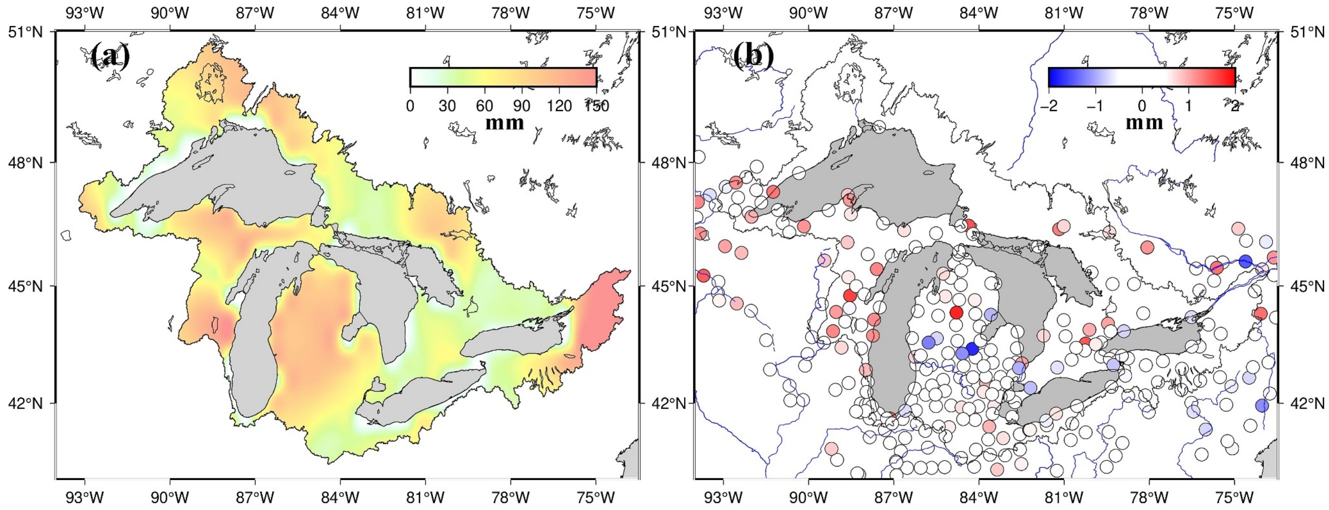

Figure 4. (a) Annual amplitudes of TWS_{GPS} on land in Great Lakes Watershed (color gradations). (b) The residuals between GPS-observed and forward-calculated displacements and the white circles indicate the absolute residual less than 0.5 mm.

between them is only 0.18 mm (Figure 4b), indicating that the applied inversion process can recover the hydrological mass loading in GLW effectively.

In this study, an available dense GPS network in Michigan has an average interstation distance of ∼30 km, which can resolve the distribution of TWS at a spatial resolution of ∼30 km. However, in other regions, reduced coverage of GPS stations would generate TWS with coarse spatial resolution relative to Michigan, especially in the northern GLW, the local features of TWS may not be recovered due to sparse distribution of GPS stations. On average, GPS can provide TWS on land in GLW with a spatial resolution of ∼45 km, almost 7× higher than that of GRACE (∼300 km).

4.3. Long-Term Changes in Total Water Storage in GLW

To approximately match the GRACE/GFO observed mass changes in GLW, we smoothed the SWS measured by water level gauges with a 300-km Gaussian filter and removed the average value from 2010 through 2020 from both time series (Figure 5). During 2010 through 2020, TWS from GRACE/GFO increased with a rate of

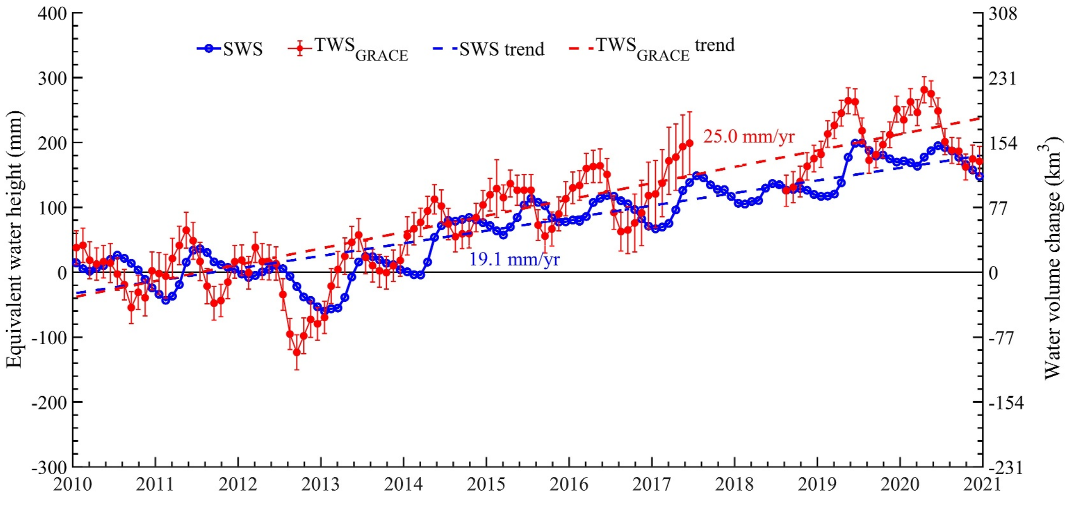

Figure 5. Total Water Storage (TWS) estimated by GRACE/GFO (red) and surface water storage measured by water level gauges smoothed by 300 km Gaussian filter (blue). Left axis presents the water height change in term of EWH (mm) and right axis indicates the corresponding water volume change (km^3). Error bars represent the uncertainties in the GRACE-derived TWS.

Table 1
Long Term Change in TWS_{GRACE}, TWS_{GPS} and TWS_{CHM} Simulated Water Storage on Land in GLW Over Different Time Spans, Unit in km^3

	2010–2020	2010–2012	2012–2020
TWS_{GRACE}	46.0	−47.0	97.0
TWS_{GPS}	83.0	−41.0	128.0
TWS_{CHM}			−41.0

25.0 ± 2.6 mm/yr, equal to a total volume of 215.0 ± 21.9 km^3; however, SWS only increased by 169.0 ± 13.2 km^3, which indicated that there was an additional water storage increase of ~46.0 km^3 on land in GLW (Table 1).

GPS-inferred TWS (TWS_{GPS}) on land (hereafter, TWS_{GPS} on land refers to TWS_{GPS}-SWS, similarly applies to TWS_{GRACE}) increased by 83.0 ± 17.9 km^3 from 2010 through 2020, which is significantly larger than GRACE/GFO estimates (~46.0 ± 12.4 km^3) (Figure 6). During 2010 through 2012, both GRACE/GFO and GPS estimates show decreasing TWS trends on land in GLW, the TWS_{GRACE} on land decreased by 47.0 ± 6.4 km^3, the TWS_{GPS} on land decreased by 41.0 ± 5.6 km^3 (Table 1). Especially in 2012, a rapid decrease appeared in TWS on land in GLW, caused by an extreme drought event with high evaporation rates due to increased temperatures and lower annual ice coverage percentage (only 13%) (Figure 1d and Figure S9 in Supporting Information S1). From 2013 through 2020, TWS_{GPS} on land increased by 128.0 ± 14.2 km^3 and TWS_{GRACE} on land increased by 97.0 ± 15.8 km^3. However, CHM estimates yielded a declining trend (−3.7 ± 1.5 km^3/yr), losing 41.0 ± 16.8 km^3 of water, which suggests the CHM significantly underestimated the long-term trend in TWS relative to GRACE and GPS results. This discrepancy may be attributed to the contribution of GWS change which is not included in the CHM data. TWS increased markedly in 2013–2014, attributing to significant increase snowfall and the relative low evapotranspiration in the basin (Figure S10 in Supporting Information S1).

To better understand TWS trends on land in GLW, we compared the spatial patterns of TWS_{GPS} trends with those estimated from GRACE (TWS_{GRACE}; Figure 7). Results show that TWS_{GPS} can capture the fine-scale local features of TWS trends on land in GLW (Figures 7a1 and 7a2). GPS derived decreasing TWS trends in the southeast Lower Peninsula of Michigan are attributed to increasing water consumption, especially during the drought period from 2010 to 2012, with depletion reaching 125.0 mm/yr. However, in northern and eastern Lake Huron, water storage increased greatly during 2010–2012 and 2013–2020 due to high snowfall. In contrast, GRACE failed to capture land water storage trends in this region during 2013–2020 and even showed the opposite trend relative to GPS results, mainly attributed to its coarse spatial resolution and signal leakage from surrounding areas. In the eastern GLW, although both GPS and GRACE show declining TWS, GRACE/GFO underestimated TWS trends relative to GPS (Figures 7a1 and 7a2 vs. 7c1 and 7c2).

To explain the discrepancy between GPS and GRACE/FO, we reprojected the 0.5° × 0.5° (~30 × 50 km) gridded TWS_{GPS} data into fully normalized spherical harmonics, truncated at degree and order 90, and applied the 300-km Gaussian smoothing filter (Figures 7b1 and 7b2). The spatial patterns of TWS trends from GPS after filtering are similar to those from GRACE/GFO estimates overall, slight differences exist in some areas (e.g., northwest and

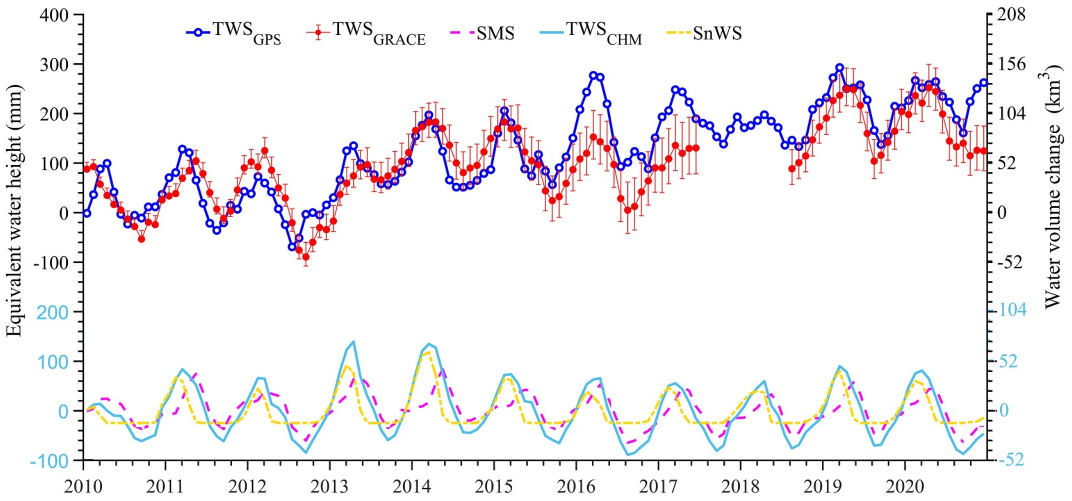

Figure 6. Monthly changes in TWS_{GPS} (blue curve), TWS_{GRACE} (after removing Great Lakes surface water via smoothing with a 300 km Gaussian filter) (red dots) and the TWS_{CHM} (cyan curve) time series. For clarity, the model data are offset to the bottom (cyan axis). The error bars represent the uncertainties in TWS_{GRACE}.

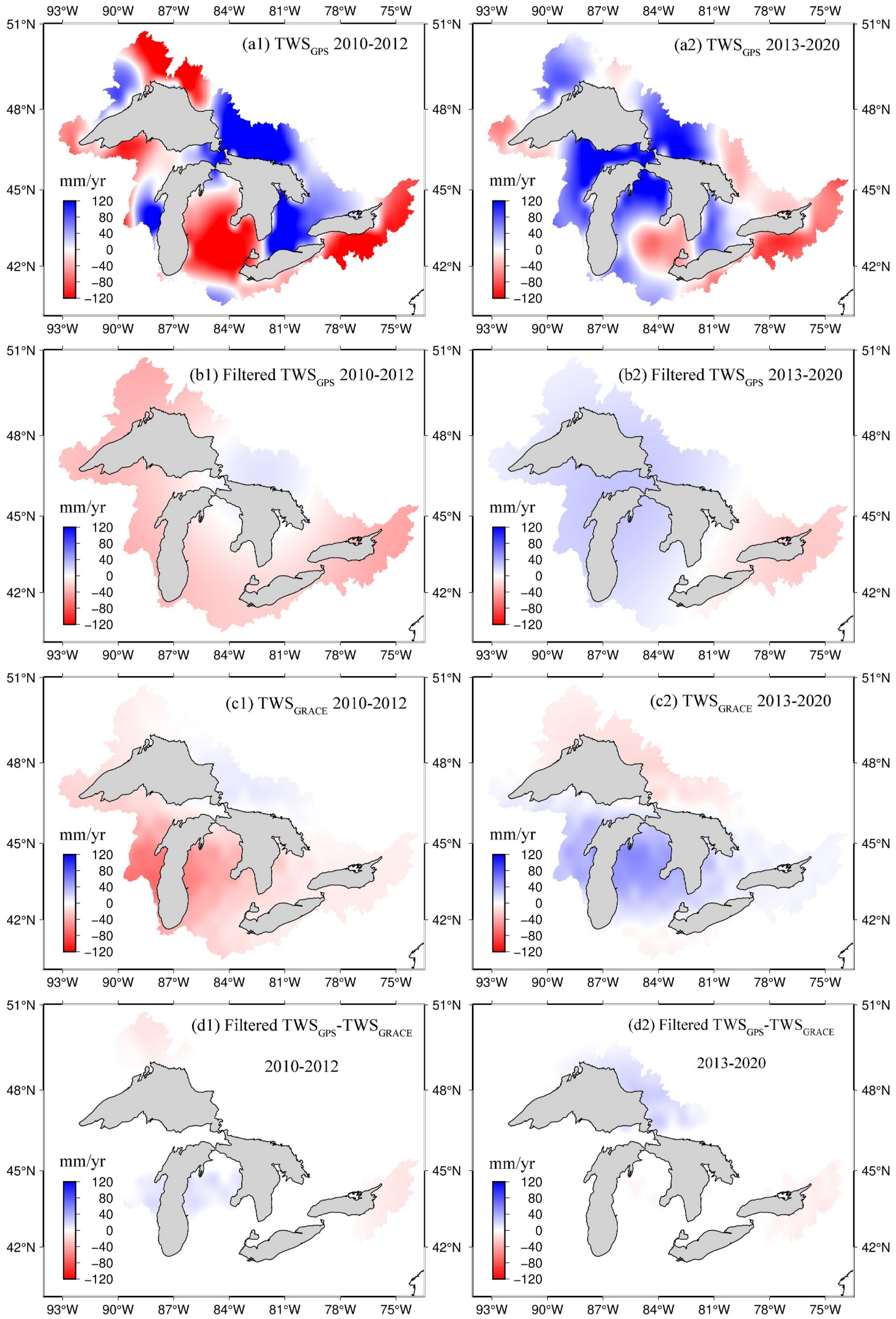

Figure 7. Left panels are long-term trends in TWS_{GPS} (a1), filtered TWS_{GPS} (b1), TWS_{GRACE} (c1) and the difference between (b1) and (c1) from 2010 through 2012. Right panels are similar to left, but for period of 2013 through 2020.

eastern GLW) (Figures 7d1 and 7d2). The possible reason for the discrepancy is that detailed water load features cannot be recovered in the northwest GLW due to the sparse distribution of GPS stations (Figures 3 and 4). In contrast, the discrepancy in eastern GLW between the TWS_{GPS} and TWS_{GRACE} on land are mainly due to GRACE/GFO largely underestimating the decreasing TWS trends; however, dense GPS station network show fully recovered TWS variations. The results confirm that dense GPS stations can show TWS variations on land in GLW with high spatial resolution and may complement the GRACE/GFO data.

4.4. Seasonal Total Water Storage Variations on Land in GLW

We first investigated annual amplitudes and phases in GPS observed vertical land motion related to seasonal oscillations in water loading in GLW. Annual amplitudes of these GPS vertical observations varied from 1.0 to 7.0 mm with a mean value of ~2.1 mm, suggesting that seasonal behavior is a dominant feature in vertical displacement in GLW (Figure 8a). In the eastern GLW, vertical displacements recorded at GPS stations peaked from July to August, while in the western region, the GPS vertical observations peaked from September to October, lagging behind those in the eastern area (Figure 8b). Some GPS stations located in the eastern GLW show phase outliers relative to nearby stations, which may be forced by strong local loading. GPS recorded vertical displacement is tightly correlated with local water storage changes, for example, vertical displacement reaches its maximum value at the time of minimum water storage. Therefore, GPS vertical position time series may provide additional insights for understanding local hydrological dynamics.

We examined the spatial distribution of seasonal water oscillations on land inferred from GPS and compared them with estimates from GRACE/GFO and CHM outputs in equivalent water thickness (Figures 8c–8g). The results indicate that spatial distribution of TWS on land from different water products generally agree with each other, all patterns show larger annual amplitudes in Michigan and in the northern area of Lake Huron than elsewhere; however, some obvious differences are found in seasonal amplitudes among these maps.

The seasonal amplitudes in TWS_{GPS} on land are substantially larger than those in TWS_{GRACE} and CHM outputs (Figures 8d and 8e) in most parts of GLW and show more fine-scale local mass change features. The average annual amplitude of TWS_{GPS} on land is ~82.0 mm (Figure 8c), which exceeds those derived from GRACE/GFO (~48.0 mm) and CHM (~62.0 mm) data sets. The maximum amplitude in the TWS_{GPS} on land was ~180 mm in the eastern GLW, greatly exceeding the amplitudes (~90.0 mm) provided by the GRACE/GFO (Figures 6c and 6d). In the northern GLW, the annual amplitude of TWS_{CHM} is similar to that from the SnWS in SNODAS (Figures 8e and 8g), which indicates that the snow mass change is a significant source of water storage, and contributes more to water storage than soil moisture (Figure 8f). One exception to these general differences is that TWS_{CHM} shows larger annual amplitudes in the northern GLW than TWS_{GRACE} and TWS_{GPS}. This discrepancy mainly arises from insufficient spatial coverage of the continuous GPS network in this area (Figures 3 and 4), which reduces its ability to adequately constrain water storage variations, and the coarse spatial resolution of GRACE/GFO data.

We further explored potential drivers of seasonal water storage variations. Due to the humid continental climate in the study area, monthly rainfall is uniformly distributed and precipitation accumulates steadily each year (Argus et al., 2020). Relationships between precipitation and TWS products from different sources (GPS, GRACE/GFO, and CHM) are relatively weak (correlation coefficients: 0.03 to 0.21). However, strong correlations (0.60–0.85) exist between monthly TWS variations from multiple water products and SnWS. Snow accumulates in autumn and winter and melts in spring, which results in SnWS peaks in March. In addition, with the relatively low temperature in these months, evaporation of the Great Lakes is significantly reduced, leading to a gradual increase in TWS on land, and consequently TWS peaks in March or April with a lag of 1–2 months w.r.t the SnWS peak (Table 2). In late spring and summer, as temperatures rise and snow melts, a portion of the water returns to the atmosphere through evapotranspiration (ET); a portion is used to supply groundwater; and the remainder discharges into the Great Lakes through runoff. Therefore, TWS on land gradually decreases and reaches to a minimum in August.

4.5. Groundwater Storage Changes in GLW

As mentioned in Section 1, the GWS is an important contributor to the TWS, but it is still not well presented quantitatively. Here following Equation 6, we calculated the GWS variations based on TWS on land from GPS, GRACE/GFO and CHM consisting of SnWS in SNODAS and SMS in NLDAS. As shown in Figure 9, the GPS

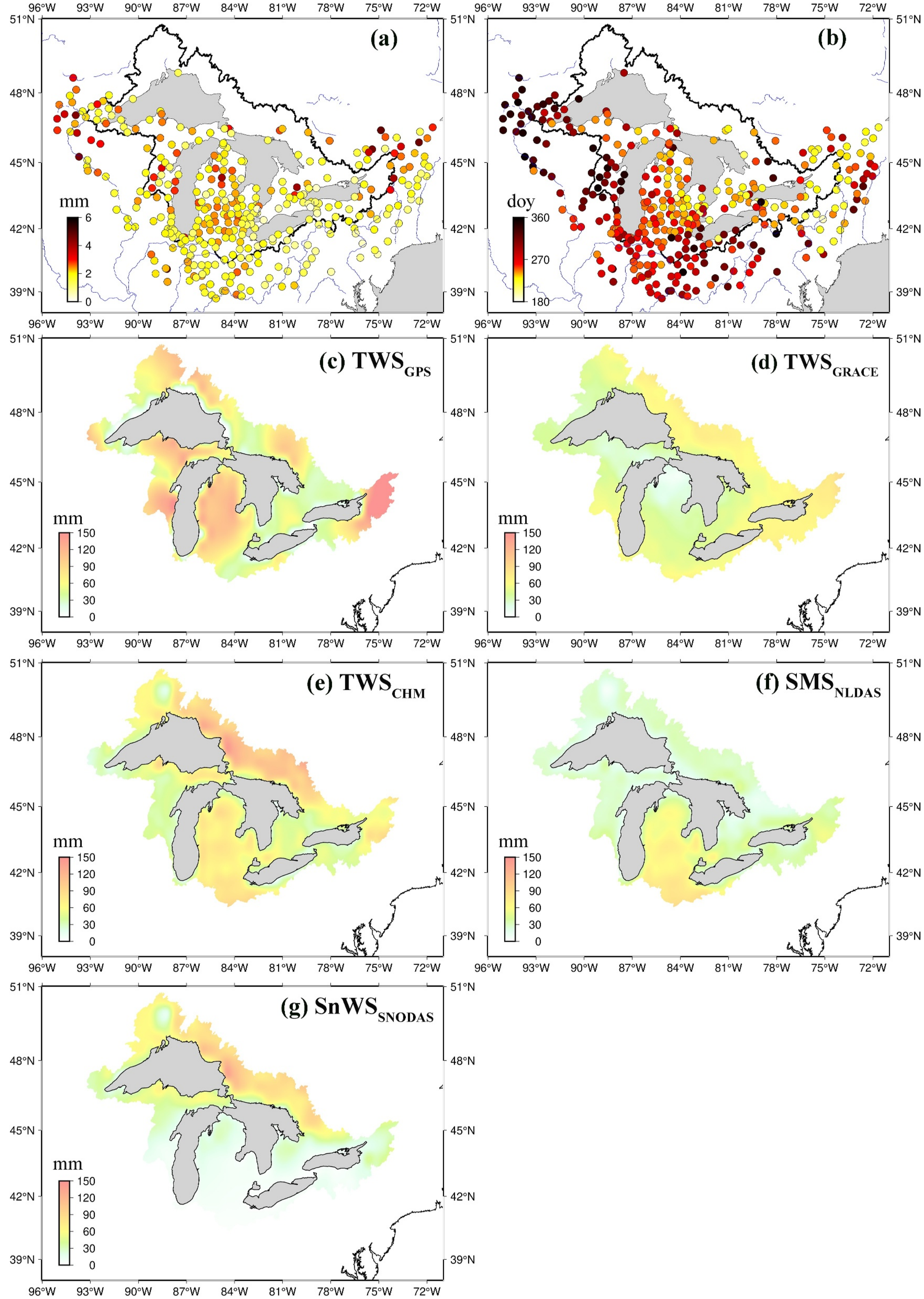
(a)
mm
(b)
doy
(c) TWS$_{GPS}$
(d) TWS$_{GRACE}$
(e) TWS$_{CHM}$
(f) SMS$_{NLDAS}$
(g) SnWS$_{SNODAS}$

Figure 8.

Table 2
Maximum Correlation Coefficients and Corresponding Phase Lags Among TWS on Land From GPS, GRACE/GFO, CHM and Precipitation (PRECI) and SnWS in GLW

	TWS_{GPS}	TWS_{GRACE}	TWS_{CHM}	PRECI	SnWS
TWS_{GPS}		0.86/1	0.76/0	0.21/−1	0.65/−1
TWS_{GRACE}			0.58/−1	0.12/−1	0.60/−1
TWS_{CHM}				0.03/0	0.85/0

based GWS estimates are in good agreement with that from GRACE/GFO at long term and seasonal time scales. GPS based GWS increased with a steady rate of 8.4 ± 1.1 km^3/yr (eqs. to 16.5 mm/yr in EWH), slightly larger than the GRACE/GFO estimated GWS trend (5.7 ± 1.2 km^3/yr, eqs. to 10.9 mm/yr in EWH) over the 2010–2020. The GWS seasonal fluctuations have peak to peak amplitude of ∼40 km^3 with the minimum and maximum appears in March and September, respectively.

We further investigated the spatiotemporal variations of GWS inferred from GPS in four subbasins of GLW associated with other water components from 2010 through 2020 (Figure 10). The results indicate that the distribution of the trends in GWS is highly heterogeneous in the four subbasins. GWS variations in subbasins A and B were dominated by long term trends, with an increasing rate of 54.9 ± 2.3 mm/yr and 51.51 ± 2.0 mm/yr, respectively (Figures 10A1 and 10B1), and GWS changes in subbasin D show large interannual variations with a slight increase of 11.8 ± 3.2 mm/yr (Figure 10D1). However, GWS in subbasin C showed a declining trend with −5.4 ± 1.6 mm/yr (Figure 10C1). On land in GLW, seasonal GWS peaks in September and has a minimum in March, and the timing of the peak behaves differently in various subbasins. In subbasins A, B, and C, GWS peaks around September (Figures 10A2 and 10B2). In subbasin D, the GWS and TWS showed good phase alignment, peaking in March (Figure 10D2). These data indicate dynamic processes in groundwater and its connection with other water components, such as snow and soil moisture.

SnWS and SMS exhibit consistency in phase across different subbasins but yet demonstrate differences in magnitude (Figures 10A2, 10B2, 10C2, and 10D2). Thick snow covers subbasins A, B, and C in winter, peaking in March, especially in subbasin A, with an annual amplitude of SnWS excess of 150.0 mm. In subbasin D, the maximum seasonal amplitude of SnWS is less than 20.0 mm and can be neglected. However, SMS has the largest amplitude in subbasin D with 120.0 mm, nearly 2 × larger than that in subbasins A, B or C.

5. Discussion and Conclusion

5.1. Assessment of Groundwater Storage Changes on Land

Based on GRACE/GFO data, Huang et al. (2012) and Argus et al. (2020) detected GWS variations on land in GLW. Huang et al. (2012) reported that a declining trend in GWS varied from 2.3 to 9.3 km^3/yr and annual amplitude varied from 14.2 to 47.6 km^3 during the 2002 to 2009 period. This discrepancy is mainly caused by the large uncertainty in SMS and SnWS outputs from different hydrological models combined with the coarse resolution of GRACE data. Argus et al. (2020) estimated that GWS increased by ∼50.0 ± 50 km^3 from 2013 to 2019 and groundwater reached a maximum with a peak-to-peak amplitude of ∼60 km^3 around March, 6 months before the lake water peaked in September. Our estimates show that during 2013–2019, GWS on land increased substantially with a total amount of 70.0 ± 22 km^3 from GPS and 63 ± 42 km^3 from GRACE/GFO. In terms of seasonal fluctuation, we found that groundwater storage increased by ∼40 km^3 in summer and fall, and decreased by an approximately equivalent amount in winter and spring. Additionally, GWS on land peaked in September with about 1 month lag behind the lake water peak, which is different to the peak time (March) given by Argus et al. (2020).

The GWS seasonal variations are driven by various seasonal factors. Precipitation in GLW is uniformly distributed over time and accumulates steadily throughout the year; however, ∼90% of snow occurs in winter and spring, accumulating on the ground in GLW and rapidly melts in April and May and remains absent until December (Figure 6 and Figure S10 in Supporting Information S1). In late spring, runoff increases with snow melting, ET in the basin is still low due to the relatively low temperatures, so a large amount of water flows into

Figure 8. Annual amplitudes (a) and phases (b) of vertical displacements recorded by 368 continuous global positioning system (GPS) stations and spatial distribution of annual Total Water Storage variations on land inferred from GPS (c), GRACE/GFO (d), composite hydrological model (e), SMS in NLDAS (f), and snow water storage in SNODAS (g) from 2010 through 2020. The annual phase presented by the day of year (doy) refers to the time of vertical deformation reaching its seasonal maximum value. Annual amplitudes of GNSS vertical displacements are low generally with an average ∼2.1 mm, the phase varies with displacements later in the year in the west and earlier in the east.

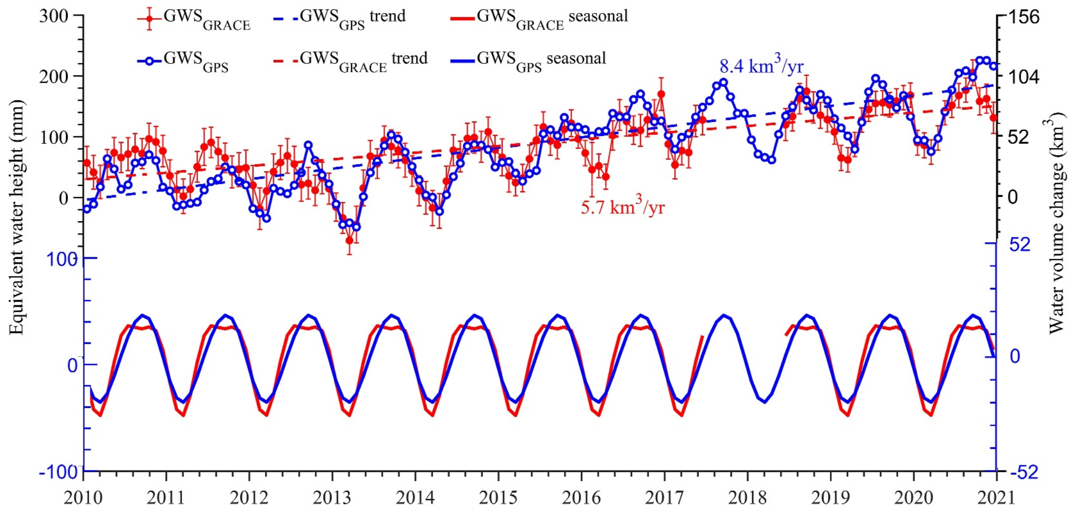

Figure 9. Temporal variations in GWS on land derived from GRACE/GFO and global positioning system (GPS). Left axis shows EWH in mm and the right axis shows the corresponding water volume change in km^3. For clarity, the seasonal term of GWS is offset to the bottom (blue axis). The vertical bars represent the uncertainties in the GWS_{GRACE}. GWS on land derived from GRACE/GFO and GPS show good agreement in the temporal pattern, reaching a maximum around September with a peak-to-peak amplitude of 40 km^3 and GWS inferred from GPS increased at a rate of 8.4 ± 1.1 km^3/yr from 2010 to 2020, slightly greater than GRACE/GFO estimates (5.7 ± 1.2 km^3/yr).

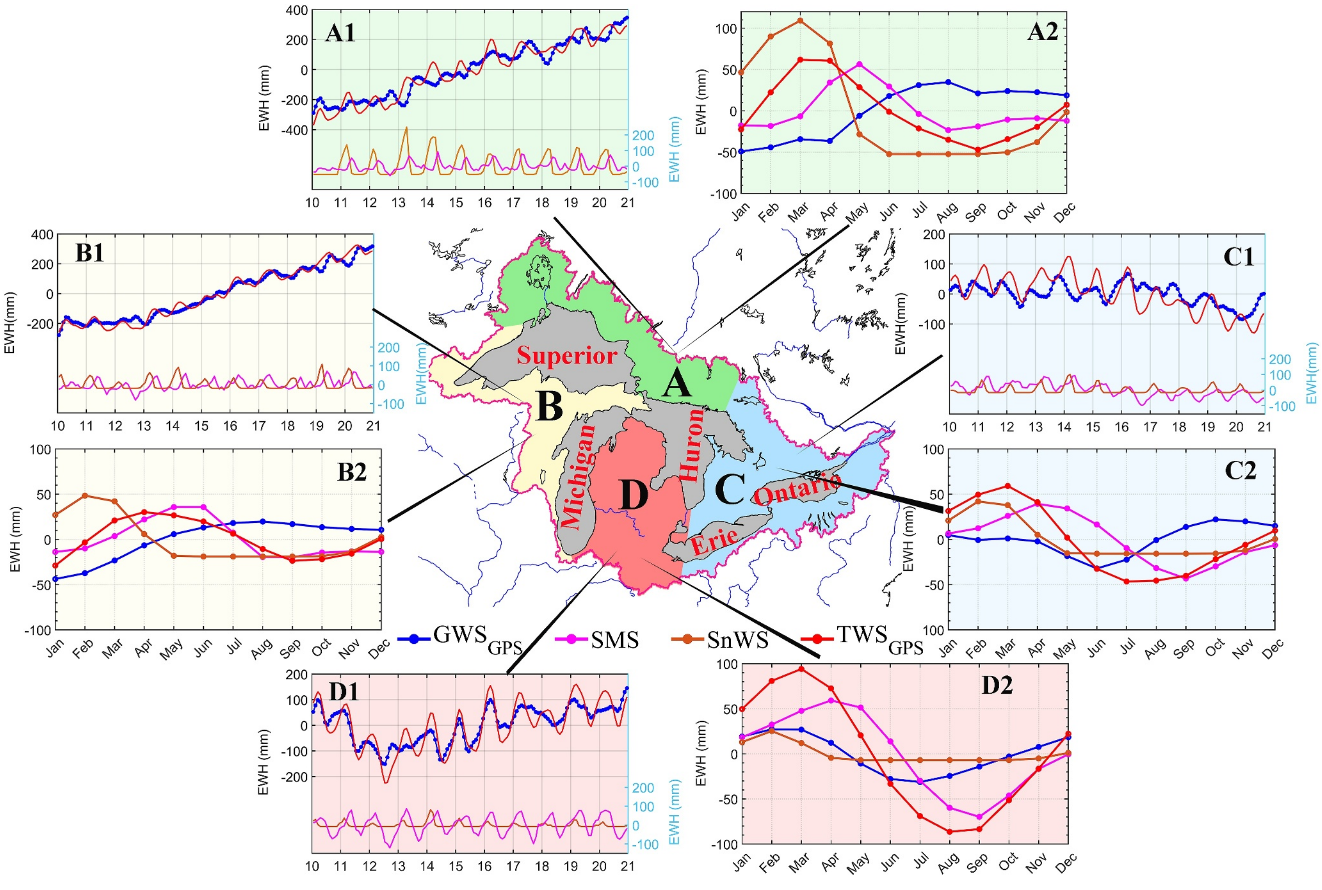

Figure 10. Monthly (A1, B1, C1, and D1) and seasonal changes (A2, B2, C2, and D2) in TWS_{GPS} (red curves), GWS_{GPS} (blue curves), SMS (pink curves) and snow water storage (SnWS) (orange curves) from 2010 through 2020 for subbasins A, B, C, and D in glw. For clarity, monthly timeseries of SMS in NLDAS and SnWS in SNODAS are offset to the base of the graphs (cyan axis).

the lakes through rivers, and the remaining water percolates through the deep soil, reaching the water table and replenishing the groundwater. Since then the GWS continually increases until reaching a maximum in September.

Due to variable snowfall patterns, runoff, soil saturation, infiltration rate and capacity, the dynamic process of GWS and transport is complex, and behaves differently in various regions of GLW. In subbasins A, B and C, the amplitudes of seasonal TWS_{GPS} on land were close to those of SnWS (Figures 10A2, 10B2, and 10C2), suggesting that snow change dominated annual TWS, resulting in a phase shift of about half a year between GWS estimates and TWS_{GPS} on land in these three basins, the GWS peaked around September. However, in subbasin D, with thinner snowpack in winter and early spring, resulting in lower snow contributions to TWS_{GPS} on land, GWS and TWS exhibited good phase alignment (Figure 10D2).

5.2. Conclusions

Based on the inversion method designed herein, the vertical displacement in the GPS data can successfully resolve spatiotemporal variations in water storage on land in GLW at monthly timescales and at 30–45 km spatial resolutions, and can effectively capture the fine-scale temporal feature of TWS on land in GLW relative to the grid spatial resolutions of GRACE/GFO mascon data (~100–300 km). GRACE/GFO largely underestimates spatial patterns of long-term trends and seasonal amplitudes in TWS on land due to its intrinsic coarse spatial resolution (~300 km) and signal leakage issues. The average annual amplitude of TWS_{GPS} on land inferred from GPS data is ~82.0 mm with a maximum amplitude of ~180.0 mm in the northeast portion of the watershed, exceeding the results estimated by CHM by 62.0 mm and GRACE/GFO by 48.0 mm. From 2010 to 2020, TWS on land inferred from GPS increased by (83.0 ± 17.9 km^3/yr) exceeded increasing TWS trends from GRACE/GFO (46.0 ± 12.4 km^3/yr). GWS changes derived from GPS are spatially heterogeneous in terms of trends in the four subbasins of the GLW, coinciding with long-term variations of TWS on land. GWS seasonal variations exhibit a half-year phase shift relative to TWS on land in the snow dominated regions (subbasins A, B and C), and have in phase change with TWS controlled by soil moisture variations (subbasin D). High-density GPS networks, where available, may serve as an independent tool to estimate high-resolution TWS variations in near real time and provide critical insights for understanding terrestrial water movement.

Data Availability Statement

The GPS daily coordinates used in this study are available from Blewitt et al. (2018). The CSR GRACE products used in the study can be publicly obtained from Save et al. (2016). The operational environmental loading products are available from (Dill & Dobslaw, 2013). Hydrologic data were downloaded from the Great Lakes Environmental Research Laboratory (GLERL) lake level products of NOAA. The NLDAS Noah LSM is available from Xia et al. (2012). ICE-6G_D (VM5a) data can be publicly obtained from Peltier et al. (2018). The SNODAS data are available from the National Operational Hydrologic Remote Sensing Center (2004).

Acknowledgments
This research was jointly supported by the Open Fund of Hubei Luojia Laboratory (220100044 and 230100016), and the NSFCs (Grants 42174042, 42174100, and 41874098).

References

Argus, D. F., Fu, Y., & Landerer, F. W. (2014). Seasonal variation in total water storage in California inferred from GPS observations of vertical land motion. *Geophysical Research Letters*, *41*(6), 1971–1980. https://doi.org/10.1002/2014gl059570

Argus, D. F., Landerer, F. W., Wiese, D. N., Martens, H. R., Fu, Y., Famiglietti, J. S., et al. (2017). Sustained water loss in California's mountain ranges during severe drought from 2012 to 2015 inferred from GPS. *Journal of Geophysical Research: Solid Earth*, *122*, 10559–10585. https://doi.org/10.1002/2017JB014424

Argus, D. F., Peltier, W. R., Blewitt, G., & Kreemer, C. (2021). The viscosity of the top third of the lower mantle estimated using GPS, GRACE, and relative sea level measurements of glacial isostatic adjustment. *Journal of Geophysical Research: Solid Earth*, *126*(5). https://doi.org/10.1029/2020JB021537

Argus, D. F., Ratliff, B., DeMets, C., Borsa, A. A., Wiese, D. N., Blewitt, G., et al. (2020). Rise of Great Lakes surface water, sinking of the upper Midwest of the United States, and viscous collapse of the forebulge of the former Laurentide ice sheet. *Journal of Geophysical Research: Solid Earth*, *125*, e2020JB019739. https://doi.org/10.1029/2020JB019739

Bierkens, M. F. P. (2015). Global hydrology 2015: State, trends, and directions. *Water Resources Research*, *51*, 4923–4947. https://doi.org/10.1002/2015WR017173

Blewitt, G., Hammond, W. C., & Kreemer, C. (2018). Harnessing the GPS data explosion for interdisciplinary science [Dataset]. *Eos*, *99*. https://doi.org/10.1029/2018EO104623

Blewitt, G., Kreemer, C., Hammond, W. C., & Argus, D. F. (2019). Improved GPS position time series spanning up to 25 years for over 18,000 stations resulting from IGS Repro 3 products, JPL's GipsyX software, and more advanced modeling techniques. In *AGU fall meeting abstracts* (Vol. 2019, p. G12A-04). American Geophysical Union.

Borsa, A. A., Agnew, D. C., & Cayan, D. R. (2014). Ongoing drought-induced uplift in the western United States. *Science*, *345*(6204), 1587–1590. https://doi.org/10.1126/science.1260279

Chen, J. L., Wilson, C. R., Tapley, B. D., Save, H., & Cretaux, J.-F. (2016). Long-term and seasonal Caspian Sea level change from satellite gravity and altimeter measurements. *Journal of Geophysical Research: Solid Earth*, *122*, 2274–2290. https://doi.org/10.1002/2016JB013595

Dill, R., & Dobslaw, H. (2013). Numerical simulations of global-scale high-resolution hydrological crustal deformations[Dataset]. *Journal of Geophysical Research: Solid Earth*, *118*, 5008–5017. https://doi.org/10.1002/jgrb.50353

ELPC (Environmental Law and Policy Center). (2019). Retrieved from https://elpc.org/wp-content/uploads/2020/04/2019-ELPCPublication-Great-Lakes-Climate-Change-Report.pdf

Enzminger, T. L., Small, E. E., & Borsa, A. A. (2018). Accuracy of snow water equivalent estimated from GPS vertical displacements: A synthetic loading case study for western U.S. Mountains. *Water Resources Research*, *54*(1). https://doi.org/10.1002/2017WR021521

Famiglietti, J. S., Cazenave, A., Eicker, A., Reager, J. T., & Velicogna, I. (2015). Satellites provide the big picture. *Science*, *349*(6249), 684–685. https://doi.org/10.1126/science.aac9238

Farrell, W. E. (1972). Deformation of the Earth by surface loads. *Reviews of Geophysics*, *10*. https://doi.org/10.1029/RG010i003p00761

Fu, Y., Argus, D. F., & Landerer, F. W. (2015). GPS as an independent measurement to estimate terrestrial water storage variations in Washington and Oregon. *Journal of Geophysical Research: Solid Earth*, *120*(1), 552–566. https://doi.org/10.1002/2014JB011415

Gronewold, A. D., Bruxer, J., Durnford, D., Smith, J. P., Clites, A. H., Seglenieks, F., et al. (2015). Hydrological drivers of record-setting water level rise on Earth's largest lake system. *Water Resources Research*, *52*, 4026–4042. https://doi.org/10.1002/2015wr018209

Harris, R. A., & Segall, P. (1987). Detection of a locked zone at depth on the Parkfield, California, segment of the San Andreas fault. *Journal of Geophysical Research*, *92*(B8), 7945–7962. https://doi.org/10.1029/JB092iB08p07945

Heki, K., & Arief, S. (2022). Crustal response to heavy rains in Southwest Japan 2017–2020. *Earth and Planetary Science Letters*, *578*. https://doi.org/10.1016/j.epsl.2021.117325

Hsu, Y. J., Fu, Y., Bürgmann, R., Hsu, S. Y., & Wu, Y. M. (2020). Assessing seasonal and interannual water storage variations in Taiwan using geodetic and hydrological data. *Earth and Planetary Science Letters*, *550*, 116532. https://doi.org/10.1016/j.epsl.2020.116532

Huang, J., Halpenny, J., van der Wal, W., Klatt, C., James, T. S., & Rivera, A. (2012). Detectability of groundwater storage change within the great lakes water basin using GRACE. *Journal of Geophysical Research*, *117*, B08401. https://doi.org/10.1029/2011JB008876

Jiang, Z., Hsu, Y. J., Yuan, L., & Huang, D. (2020). Monitoring time-varying terrestrial water storage changes using daily GNSS measurements in Yunnan, southwest China. *Remote Sensing of Environment*, *254*, 112249. https://doi.org/10.1016/j.rse.2020.112249

Jiang, Z., Hsu, Y.-J., Yuan, L., Yang, X., Ding, Y., Tang, M., & Chen, C. (2021). Characterizing spatiotemporal patterns of terrestrial water storage variations using GNSS vertical data in Sichuan, China. *Journal of Geophysical Research: Solid Earth*, *126*(12), e2021JB022398. https://doi.org/10.1029/2021JB022398

Khandelwal, A., Karpatne, A., & Ravirathinam, P. (2022). ReaLSAT, a global dataset of reservoir and lake surface area variations. *Scientific Data*, *9*, 356. https://doi.org/10.1038/s41597-022-01449-5

Knappe, E., Bendick, R., Martens, H. R., Argus, D. F., & Gardner, W. P. (2019). Downscaling vertical GPS observations to derive watershed-scale hydrologic loading in the northern Rockies. *Water Resources Research*, *55*, 391–401. https://doi.org/10.1029/2018WR023289

Li, J., Zhan, W., Guo, B., Li, S., & Guo, B. (2021). Combination of the Levenberg–Marquardt and differential evolution algorithms for the fitting of postseismic GPS time series. *Acta Geophysica*, *69*, 405–414. https://doi.org/10.1007/s11600-021-00556-y

Meredith, D. (1975). Temperature effects on great lakes water balance Studies1. *Jawra Journal of the American Water Resources Association*, *11*(1), 60–68. https://doi.org/10.1111/j.1752-1688.1975.tb00660.x

Michalak, A. (2017). Environmental sciences: Troubled waters on the great lakes. *Nature*, *543*, 488–489. https://doi.org/10.1038/543488a

Milliner, C., Materna, K., Bürgmann, R., Fu, Y., Moore, A. W., Bekaert, D., et al. (2018). Tracking the weight of Hurricane Harvey's stormwater using GPS data. *Science Advances*, *4*(9), eaau2477. https://doi.org/10.1126/sciadv.aau2477

Mitchell, K. E., & Kenneth, E. (2004). The multi-institution North American Land Data Assimilation System (NLDAS): Utilizing multiple GCIP products and partners in a continental distributed hydrological modeling system. *Journal of Geophysical Research*, *109*(D7), 585–587. https://doi.org/10.1029/2003JD003823

Nahmani, S., Bock, O., Bouin, M. N., Santamaría-Gómez, A., Boy, J. P., Collilieux, X., et al. (2012). Hydrological deformation induced by the west African Monsoon: Comparison of GPS, GRACE and loading models. *Journal of Geophysical Research*, *117*(B5), B05409. https://doi.org/10.1029/2011jb009102

National Operational Hydrologic Remote Sensing Center. (2004). Snow data assimilation system (SNODAS) data products at NSIDC, Version 1 [Dataset]. *Boulder, Colorado USA. National Snow and Ice Data Center*. https://doi.org/10.7265/N5TB14TC

Overacker, J., Hammond, W. C., Blewitt, G., & Kreemer, C. (2022). Vertical land motion of the high plains aquifer region of the United States: Effect of aquifer confinement style, Climate variability, and anthropogenic activity. *Water Resources Research*, *58*(6), e2021WR031635. https://doi.org/10.1029/2021wr031635

Peltier, R. W., Argus, D. F., & Drummond, R. (2018). Comment on "an assessment of the ice-6g_c (vm5a) glacial isostatic adjustment model" by purcell et al. *Journal of Geophysical Research: Solid Earth*, *123*(2), 2019–2028. https://doi.org/10.1002/2016JB013844

Rodell, M., Famiglietti, J. S., Wiese, D. N., Reager, J. T., Beaudoing, H. K., Landerer, F. W., et al. (2018). Emerging trends in global freshwater availability. *Nature*, *557*, 651–659. https://doi.org/10.1038/s41586-018-0123-1

Save, H. (2019). CSR GRACE RL06 Mascon solutions [Dataset]. *Texas data repository Dataverse*, *V1*. https://doi.org/10.18738/T8/UN91VR

Save, H., Bettadpur, S., & Tapley, B. D. (2016). High resolution CSR GRACE RL05 mascons. *Journal of Geophysical Research: Solid Earth*, *121*, 7547–7569. https://doi.org/10.1002/2016JB013007

Scanlon, B. R., Zhang, Z., Save, H., Sun, A. Y., Schmied, H. M., Beek, L. V., et al. (2018). Global models underestimate large decadal declining and rising water storage trends relative to GRACE satellite data. *Proceedings of the National Academy of Sciences of the United States of America*, *115*(6), E1080–E1089. https://doi.org/10.1073/pnas.1704665115

Tapley, B. D., Bettadpur, S., Watkins, M. M., & Reigber, C. (2004). The gravity recovery and climate experiment: Mission overview and early results. *Geophysical Research Letters*, *31*, L09607. https://doi.org/10.1029/2004GL019920

Tapley, B. D., Watkins, M. M., Flechtner, F., Reigber, C., Bettadpur, S., Rodell, M., et al. (2019). Contributions of GRACE to understanding climate change. *Nature Climate Change*. https://doi.org/10.1038/s41558-019-0456-2

Wahr, J., Khan, S. A., Van Dam, T., Liu, L., Van Angelen, J. H., Van, d. B., et al. (2013). The use of GPS horizontals for loading studies, with applications to northern California and southeast Greenland. *Journal of Geophysical Research: Solid Earth*, *118*(4). https://doi.org/10.1002/jgrb.50104

Wang, L., Bevis, M., Peng, Z., Kaban, M. K., Thomas, M., & Chen, C. (2022). Tracking the source direction of surface mass loads using vertical and horizontal displacements from satellite geodesy: A case study of the inter-annual fluctuations in the water level in the great lakes. *Remote Sensing of Environment*, *274*, 113001. https://doi.org/10.1016/j.rse.2022.113001

White, A. M., Gardner, W. P., Borsa, A. A., Argus, D. F., & Martens, H. R. (2022). A review of GNSS/GPS in hydrogeodesy: Hydrologic loading applications and their implications for water resource research. *Water Resources Research*, *58*, e2022WR032078. https://doi.org/10.1029/2022WR032078

Xia, Y., Mitchell, K., Ek, M., Sheffield, J., Cosgrove, B., Wood, E., et al. (2012). Continental-scale water and energy flux analysis and validation for the North American land data assimilation system project phase 2 (NLDAS-2): 1. Intercomparison and application of model products [Dataset]. *Journal of Geophysical Research*. https://doi.org/10.1029/2011JD016048

Xue, L., Fu, Y., & Martens, H. R. (2021). Seasonal hydrological loading in the great lakes region detected by GNSS: A comparison with hydrological models. *Geophysical Journal International*, *226*, 1174–1186. https://doi.org/10.1093/gji/ggab158

Yan, J., Dong, D., Bürgmann, R., Materna, K., Tan, W., Peng, Y., & Chen, J. (2019). Separation of sources of seasonal uplift in China using independent component analysis of GNSS time series. *Journal of Geophysical Research: Solid Earth*, *124*, 11951–11971. https://doi.org/10.1029/2019JB018139

Young, Z. M., Kreemer, C., & Blewitt, G. (2021). GPS constraints on drought-induced groundwater loss around Great Salt Lake, Utah, with implications for seismicity modulation. *Journal of Geophysical Research: Solid Earth*, *126*, e2021JB022020. https://doi.org/10.1029/2021JB022020

Zhang, L., Tang, H., & Sun, W. (2021). Comparison of GRACE and GNSS seasonal load displacements considering regional averages and discrete points. *Journal of Geophysical Research: Solid Earth*, *126*(8), 1–27. https://doi.org/10.1029/2021JB021775